2012

Impact fragmentation of aluminum reactive materials

Hooper, J.P.

J. P. Hooper. "Impact fragmentation of aluminum reactive materials." J. Appl. Phys. 112, 043508 (2012).
https://hdl.handle.net/10945/52008

Impact fragmentation of aluminum reactive materials

Joseph P. Hooper[a)]
Department of Physics, Naval Postgraduate School, Monterey, California 93943, USA

(Received 30 March 2012; accepted 17 July 2012; published online 24 August 2012)

We report the fragmentation of brittle, granular aluminum spheres following high velocity impact (0.5-2.0 km/s) on thin steel plates. These spheres, machined from isostatically pressed aluminum powder, represent a prototypical metallic reactive material. The fragments generated by the impacts are collected in a soft-catch apparatus and analyzed down to a length scale of 44 μm. With increasing velocity, there is a transition from an exponential Poisson-process fragment distribution with a characteristic length scale to a power-law behavior indicative of scale-invariance. A normalized power-law distribution with a finite size cutoff is introduced and used to analyze the number and mass distributions of the recovered fragments. At high impact velocities, the power-law behavior dominates the distribution and the power-law exponent is identical to the universal value for brittle fragmentation discussed in recent works. The length scale at which the power-law behavior decays is consistent with the idea that the length of side microbranches or damage zones from primary cracks is governing this cutoff. The transition in fragment distribution at high strain-rates also implies a significant increase in small fragments that can rapidly combust in an ambient atmosphere.
[http://dx.doi.org/10.1063/1.4746788]

I. INTRODUCTION

The fragmentation of brittle materials has recently received considerable attention due to both pragmatic interests in material failure as well as the scale-invariant behavior observed in brittle fragment distributions. In this work, we focus on the failure properties of brittle reactive materials; these compounds, inert under normal conditions, combust rapidly under intense dynamic loading from a shock wave or high-velocity impact.[1–4] Many reactive material formulations are designed to fragment heavily under high strain-rate loading, resulting in a combustible metal debris cloud. The fragmentation properties of such materials are key to their ultimate combustion behavior, but little is currently known about their dynamic failure.

There is also considerable interest in the basic form of the fragment distribution of brittle materials. These distributions differ from those observed in metals and other ductile materials, which are often characterized by an exponential distribution with a characteristic length scale. Exponential type forms for fragmenting metals are generally considered to arise from uncorrelated nucleation of failure points or cracks governed by Poisson statistics. The distributions of Grady and Kipp[5,6] and Mott and Linfoot[7] are widely used for high strain-rate fragmentation processes in which there is a characteristic length or mass scale.

In the case of brittle materials, a power-law rather than an exponential form is frequently observed.[8–14] This corresponds to a regime in which the fragment distribution has certain aspects of scale-invariance and can be treated as a fractal with a particular dimensionality. Oddershede and coworkers suggested that the power-law behavior observed in brittle fragment distributions could be interpreted in the context of self-organized criticality, and proposed a fragment distribution of the form,

$$N(m) \propto m^{-D_f} \exp(-m/m_o),$$

describing the complementary cumulative distribution of fragment number N over the fragment mass m with a finite size cutoff m_o. A relation between the shape of the material and the fractal dimension D_f was introduced and shown to hold for a wide range of morphologies.[8]

Many authors have subsequently examined the statistical nature of brittle fragmentation, including a number of discussions of universality in the power-law exponent.[9] A recent review by Åström discusses much of the relevant analysis in this area.[15] Several authors have had success in interpreting brittle fragmentation patterns using a combined exponential and power-law form to treat large and small fragments, respectively.[9,16] The statistics of the fragment pattern provides only indirect information on the mechanism, but recent work has suggested that the fractal behavior may arise from the microbranching of high-velocity cracks.[17–19] Sharon and Fineberg report increasing side-branch lengths as the crack velocity approaches the limiting Rayleigh wave speed, suggesting that higher rates of loading may lead to an increase in the amount of material affected by the side branching.[17,20,21] Fineberg and Marder reviewed the large body of recent work on microbranching of fast-running cracks in brittle materials.[22]

The majority of experimental brittle fragmentation studies have focused on low velocity impact of samples, often by dropping or crushing. In order to examine the evolution of the fragment distribution of a brittle reactive material under high strain-rate loading, we have performed high-velocity impact experiments in which isostatically pressed granular aluminum spheres were fired from a powder gun into a thin

a)Electronic mail: jphooper@nps.edu.

steel plate. The spheres fully perforated the plate and were heavily fragmented in the process; the resulting debris cloud was caught in a soft-catch apparatus and analyzed.

These experiments reveal a transition from an exponential type distribution at low velocity impact (610 m/s) to power-law behavior at higher velocities approaching 2 km/s. The power-law exponent is, in all cases, very close to the universal value for three-dimensional fragments suggested in recent work.[9] We introduce a normalized power-law distribution with a finite size cutoff which is used to analyze the mass distribution over a linear fragment scale. This form provides a very good description of experimental data at high impact velocities, and at the lowest velocity it was combined with a standard exponential form to model the behavior. We also consider simple ways to estimate the physical parameters appearing in the theoretical forms. The fragment distributions presented here provide a basis for analyzing the combustion damage from reactive material debris clouds.

II. EXPERIMENTAL

Spherical porous aluminum projectiles 2.51 cm in diameter were cut from a cylinder of Valimet H-2 aluminum powder which had been isostatically pressed into a monolith at 20 ksi at ambient temperature. The resulting density of the porous aluminum was 2.39 g/cc (about 15% porosity). No detailed measurements of the fracture toughness were made, but a simple Brazilian crush test on this material gave a tensile strength of 8.27 MPa, two orders of magnitude lower than standard 6061 aluminum. These spheres were then fired at a thin steel plate using saboted launchers from a 42 mm smooth-bore powder gun at Naval Surface Warfare Center, Indian Head Division. Additional details of the experimental setup can be found in Ref. 23. High speed video was used to ensure that the spheres remained coherent before impact. Target muzzle velocities of the spheres were 610 m/s, 1220 m/s, and 1829 m/s, and were measured using a laser velocimeter at the end of the gun barrel. Actual projectile velocities were within ± 10 m/s of the target velocity. Projectiles impacted three thicknesses (0.912, 1.52, and 3.04 mm) of 1018 steel plates bolted to a supporting steel frame. Relevant material properties of the impact plate and the porous aluminum projectile are given in Table I, and the various shot configurations are listed in Table II. For the two thinnest plates, projectiles fully perforated and fragmented into a debris cloud inside the chamber. For the 3.04 mm plate, shots at the two lowest velocities were sufficiently close to the ballistic limit that incomplete perforation was observed and the majority of the sphere mass was in a single large fragment on the impact side of the plate. The debris field from successful perforation events was caught in a 1.5 m sonotube filled with low-density shaving cream directly behind the impact plate. Following each shot, the shaving cream was washed from the tube with water and the remaining fragments were fed through a sieve stack to measure the mass distribution over linear particle size. Particles were sieved down to a size of 44 μm, which was sufficient in all cases to recover approximately 90% or more of the original sphere's mass. A small amount of mass (less than 2%) was lost during the sieving process. A magnet was used to remove any steel fragments that were extracted from the catch tube; the steel was generally far larger than the fragmented aluminum and was easily identified and removed. The vibration of the sieve shaker was sufficient to break up any aluminum particles that may have agglomerated in the foam.

TABLE I. Material properties of the porous, pressed aluminum projectiles, and the steel impact plate.

Property	Value
Mean aluminium powder diameter	3.2 μm
Projectile density	2.39 g/cc
Projectile diameter	2.51 cm
Projectile tensile strength	8.27 MPa
Projectile sound speed	5430 m/s
Plate density	7.85 g/cc
Plate sound speed	5900 m/s

Spall-related fragmentation is expected to play a minimal role in these experiments, in contrast to hypervelocity impact of fully densified metals. Due to the thin impact plates and the porosity of the aluminum, the shock wave induced in the sphere from the impact will be attenuated heavily by the porosity and rapidly overtaken by rarefaction waves generated at the impact plate's back surface. The majority of fragmentation is, thus, expected to arise from lateral tensile expansion of the sphere as it compresses against the plate and from inward crack propagation as the sphere deforms and perforates the steel. Additionally, we observed no evidence that aluminum fragments reacted heavily following this initial impact. Fragments were sharp and three-dimensional and showed no signs of melting or widespread conversion to oxide products. High-speed video showed a brief impact flash when spheres struck the steel plate, but no visible reaction following perforation. Thus, while we cannot fully exclude that some aluminum combustion is occurring during the soft-catch process, our data suggests it is likely minimal. Separate experiments in which the fragment cloud impacted a second thick steel plate (similar to the setup in Ref. 4) did result in significant combustion, but in this work we only consider the fragmentation from the initial thin-plate perforation.

TABLE II. Exponents and fit parameters for all fragment distributions.

Power-law (Eq. (1))			
Configuration	α	κ	$1/\beta$ (mm)
0.912 mm, 1220 m/s	0.05	1.65	1.89
0.912 mm, 1829 m/s	0.03	1.66	0.94
1.52 mm, 1220 m/s	−0.06	1.69	2.58
1.52 mm, 1829 m/s	0.07	1.64	0.83
3.04 mm, 1829 m/s	0.05	1.65	1.58
Combined exponential and power-law (Eq. (4))			
Configuration	Γ	μ (mm)	$1/\beta$ (mm)
0.912 mm, 610 m/s	0.02	0.72	0.23
1.52 mm, 610 m/s	0.01	0.87	0.40

III. RESULTS AND DISCUSSION

We first consider the raw probability density functions (PDFs) of fragment mass distributed over a linear sieve size s. The recovered fragments were run through a series of increasingly fine sieves on a sieve shaker table, and the final sample mass in each sieve was measured. Masses were converted into a piecewise continuous probability density function in which each sieve covered the range of length scales between itself and the next larger sieve. Data points for the experimental probability density functions are given at the midpoint of each sieve range. Experimental points are normalized to the total amount of mass collected for each individual shot. As 90% or greater of the original sphere mass was recovered, we do not expect additional significant features in the size range between our smallest sieve (44 μm) and the original particle size of the pressed aluminum (3.2 μm).

The data for impact on the thinnest plate, 0.912 mm, are shown in Figures 1 and 2. Solid lines represent fits to theoretical forms, which are discussed below. At low velocities, there is a distinct maximum in the fragment distribution, and the overall form is that of an exponential distribution with a characteristic length scale. At higher impact velocities, the maximum disappears and behavior consistent with a power-law distribution emerges; below approximately 1 mm, the fragment PDF is nearly constant on a logarithmic scale. The smallest fragments in the low velocity impact shot also deviate from the exponential form and show a small region of power-law type behavior, suggesting a mixture of the two distributions is already occurring at an impact velocity of 610 m/s. The very largest fragments, in the size range of 0.7 to 1.0 cm, are generally large mass chunks from the initial impact point of the sphere and deviate slightly from the overall fragment trend. The vast majority of the collected mass is below 1 mm for all shots.

In Figures 3 and 4, we present analogous plots for a thicker impact plate (1.52 mm), and the results are similar. As would be expected, the total mass contained in the largest fragments is reduced; the remainder of the fragment PDF is very similar to the thinner plate, however. An exponential form is present at the lowest impact velocity, giving way to a power-law behavior at maximum velocity. At the largest plate thickness, 3.04 mm, only the highest impact velocity (1829 m/s) resulted in a clean perforation and fragmentation. The data sets from all 1829 m/s impacts are shown in Figure 5. Save for some variation in the very largest fragments, the fragmentation patterns are quite similar; all are constant over approximately 1.5 decades of fragment size, down to the smallest size scale measured. In all systems, this behavior then decays above a cutoff value on the order of 1 mm.

Brittle fragment distributions are frequently presented in the form of fragment number distributed over mass or volume, $n(m)$ or $n(v)$. For brittle materials with a power-law distribution, Åström and coworkers have suggested the general form,

$$n(v) \propto v^{-\kappa} f(\beta v),$$

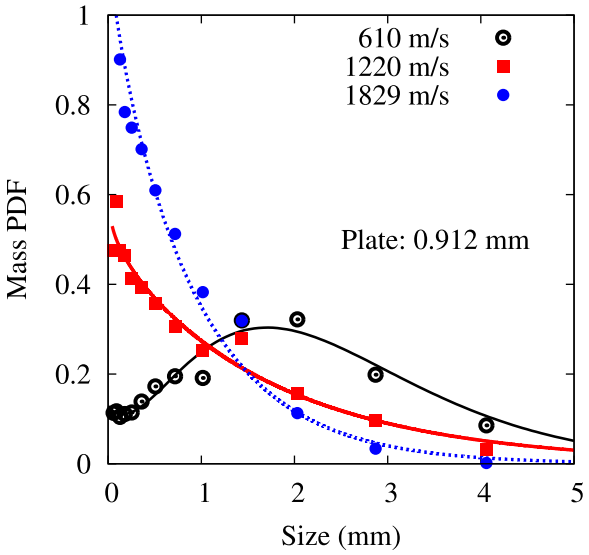

FIG. 2. Linear-scale mass PDF for impact on a 0.912 mm plate.

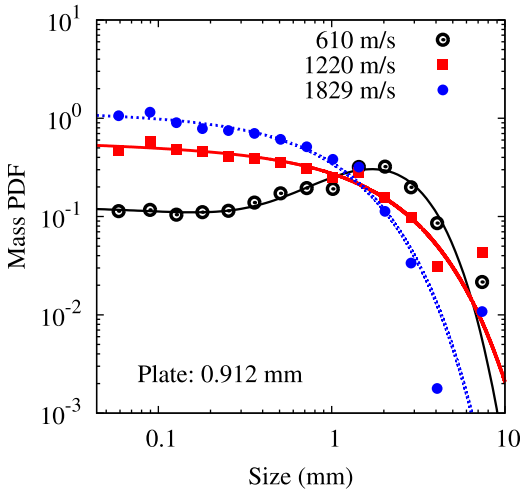

FIG. 1. Mass probability density function for fragments generated by impact and perforation of a 0.912 mm plate. Fits are based on Eqs. (1) and (4) and are described in the text.

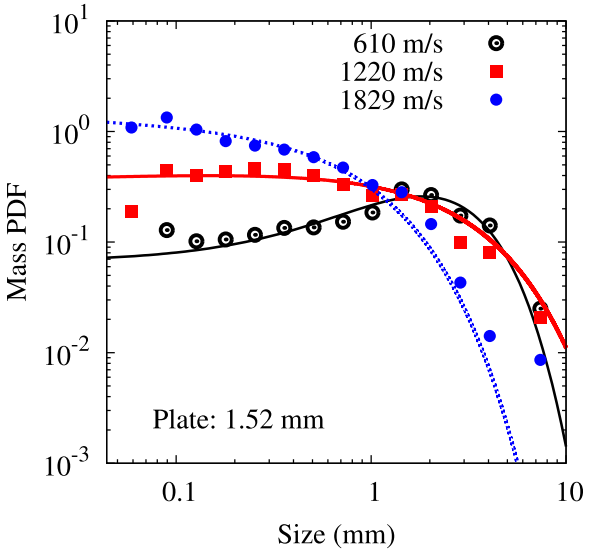

FIG. 3. Mass PDF for fragments generated by impact and perforation of a 1.52 mm plate.

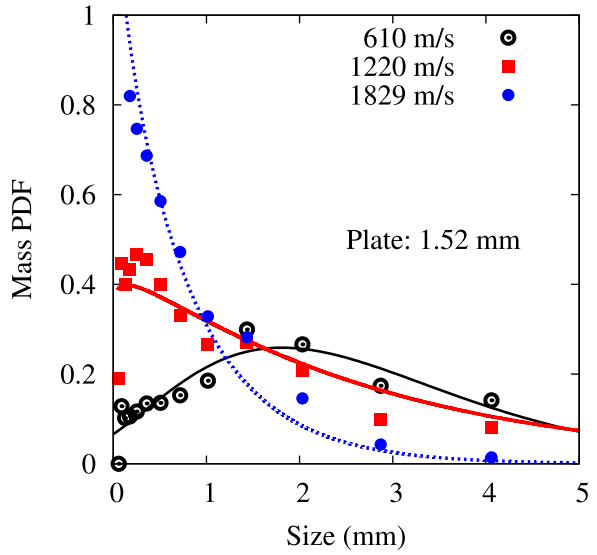

FIG. 4. Linear-scale mass PDF for impact on a 1.52 mm plate.

describing the number distribution of particles over the volume v. The function f is a damping function that cuts off the power-law behavior above some length scale governed by β. Frequently $f = \exp(-\beta v)$ is used, consistent with the original form of Oddershede and coworkers.[8] Assuming a size-independent aspect ratio of unity, recasting this form into a distribution of fragment number over linear size s yields

$$n(s) \propto s^{D-(D\kappa+1)} \exp\left(-(\beta s)^D\right),$$

where D is the dimensionality of the fragmenting object. As discussed in Ref. 9, there is flexibility in the choice of the damping function. In the general case, the above form could be combined with some manner of exponential distribution to fit a broad range of results if portions of the fragment cloud are still mainly governed by a Poisson crack nucleation process. For our data, few large fragments are found at high impact velocities, and it is unnecessary to use a separate

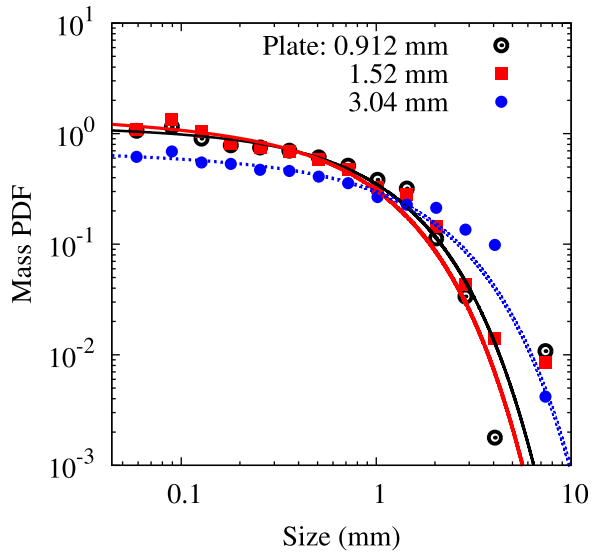

FIG. 5. Mass PDF for impact at 1829 m/s on plates of varying thickness.

distribution to fit these. Instead, we utilize the flexibility in the damping function so that a single form covers the power-law behavior (which is the majority of the mass) and also incorporates the effect of a small number of larger fragments. We thus use a form corresponding to

$$n(v) \propto v^{-\kappa} \exp\left(-(\beta v)^{\frac{1}{D}}\right).$$

The linear scale is the most relevant for data from a sieving process. Assuming that $v = s^D$, where s is a linear size of our three-dimensional fragment, we have

$$n(s) \propto s^{D-(D\kappa+1)} \exp(-\beta s),$$

where β is, as above, a damping constant that cuts off the power-law behavior at larger sizes.

The majority of the fragment mass at the higher impact velocities is well below 1 mm, and counting fragments in this size range is not viable experimentally. Instead, we convert the fragment number distributions to mass distributed over a linear length scale using the relation

$$dM = mdN = \rho s^D N_o n(s) ds,$$

where M is the cumulative mass distribution function (CDF) and N_o is the total number of fragments. Based on the above expressions, we introduce our final form for the fragment distribution, suitable for direct comparison with a full normalized distribution from the experimental sieve data

$$m(s) = \frac{1}{s_o}\left(\frac{s}{s_o}\right)^{-\alpha} \frac{\exp(-\beta s)}{E_\alpha(\beta s_o)}, \tag{1}$$

where β is a constant controlling the cutoff of the power-law behavior, s_o is a minimum fragment size, and $E_\alpha(x)$ is the generalized exponential integral function

$$E_n(x) = \int_1^\infty \frac{\exp(-xt)}{t^n} dt.$$

This form is normalized with respect to the total mass. The true minimum fragment size for our materials is likely equal to the original particle size in the pressed granular aluminum (3.2 μm); however, since the majority of the original sphere's mass is recovered in the sieving process, for simplicity, we set s_o equal to the smallest sieve, 44 μm. The cumulative distribution function corresponding to the PDF in Eq. (1) is

$$M(s) = 1 - \left(\frac{s}{s_o}\right)^{1-\alpha} \frac{E_\alpha(\beta s)}{E_\alpha(\beta s_o)}. \tag{2}$$

This represents the percent of fragment mass equal to or smaller than a linear size scale s. The term α in Eqs. (1) and (2) is related to the exponent κ used by Åström and coworkers via the relation

$$\alpha = 2D - (D\kappa + 1).$$

Based on self-similar crack branching arguments, several authors have suggested a universal value of the form

$\kappa = (2D-1)/D$, where D is the dimensionality.[9,15,24,25] The corresponding fragment mass distribution exponent α in Eq. (1) in this case would be exactly zero, and the fragment *number* distribution $n(s)$ would be a power-law of the form s^{-D}. For $\alpha = 0$, the above mass distribution reduces to a simple shifted exponential

$$m(s) = \beta \exp(-\beta(s - s_o))$$
$$M(s) = 1 - \exp(-\beta(s - s_o)), \quad (3)$$

for the PDF and CDF, respectively. For $\beta s \ll 1$ (i.e., for small fragments), this reduces to the empirical Gaudin-Schuhmann type cumulative mass distribution function

$$\frac{M(s)}{M_o} \propto (\beta s)^n,$$

where n is close to one and M_o is the total fragment mass.[26–28] This behavior has been observed experimentally in a number of brittle fragmentation experiments.[8,9,12,29]

In this situation where the number distribution of fragments has a power-law exponent equal to the "universal" value, the corresponding mass distribution $m(s)$ consists of a flat region on a log-log scale below $1/\beta$, decaying as the size approaches $1/\beta$. All our experimental shots converge to this behavior at high velocities (see Figure 5), indicating that in all cases the fragment distribution is consistent with the universal exponent discussed above. We again note that values of α close to zero (such as we observe at high strain rates) give an exponential type function for the mass distribution; this, however, corresponds to a non-exponential, power-law form when converted to the traditional fragment number distribution that most authors present. Smaller fragments in the 610 m/s impact velocity experiments also show evidence of a region at small particle sizes, where the power-law term is applicable and α is approximately zero.

The fit parameters using the above theoretical form are given in Table II, along with the corresponding value of κ which is identical to that used in the previous works.[9,15] Fits are performed with a standard least-squares analysis using the Levenberg-Marquardt algorithm. Our collected fragments have a three-dimensional character, for which the proposed universal value κ is 5/3.

At the lowest impact velocity, a power-law form does not provide a suitable fit for the entire experimental data, which shows a clear characteristic length scale. For these velocities, we find excellent agreement using a combination of an exponential form with the above power-law distribution for small fragments. In the previous work, it has been suggested that physically this could arise from Poisson nucleation of main cracks combined with power-law regions due to microbranches off these primary cracks.[15] To treat the main cracks, we introduce a standard exponential form, the Mott distribution,[6,7] for fragment number over mass for a three-dimensional object,

$$n(m) = \frac{1}{3m}\left(\frac{m}{\mu}\right)^{\frac{1}{3}} \exp\left(-\left(\frac{m}{\mu}\right)^{\frac{1}{3}}\right).$$

Converting this to a mass distribution over a linear length scale yields, for 3D fragmentation,

$$m(s) = \frac{1}{6\mu}\left(\frac{s}{\mu}\right)^3 \exp(-s/\mu).$$

For suitable fits, we combine the Mott form with our expression in Eq. (1) for the 610 m/s shots

$$m(s) = \Gamma\beta \exp(-\beta(s - s_o)) + (1-\Gamma)\frac{1}{6\mu}\left(\frac{s + 2/\beta}{\mu}\right)^3 \exp\left[-\left(\frac{s + 2/\beta}{\mu}\right)\right]. \quad (4)$$

Here, Γ provides the normalization between the two distributions. In the combined expressions, the size of the fragments in the exponential distribution is reduced by $2/\beta$, which corresponds physically to the Poisson fragment being reduced by microbranching or damage regions near the crack surface. The relationship between Γ and β is likely complex; in the simplest case, as $1/\beta$ increases the region of the material affected by the microbranches grows and Γ also increases. However, in the case of our impact fragmentation events, there is also spatial inhomogeneity of crack velocity and strain rate in the sample to consider. Certain cracks may be driven hard enough to branch extensively, but this may only be occurring in relatively small regions of the sample such as near the impact plate.

We next consider the parameter $1/\beta$, which may be interpreted as a characteristic length scale for which the power-law behavior is observed. As discussed above, several authors have suggested that this cutoff is related to the maximum length that microbranches can extend from a main crack. As pointed out by Bouchbinder and Procaccia, it is very likely that there is significant material dependence wrapped up in this parameter, and there may be no universal behavior.[30,31] They note specific differences in the brittle fragmentation of PMMA versus soda-lime glass as a representative example. In our case, however, there exists a distinct upper bound if we assume that a Poisson nucleation process for main cracks is still occurring at high impact velocities, and that the scale-invariant behavior is arising from damage zones during repeated microbranching. Since the fracture surface energy is low for our pressed aluminum spheres and the impact conditions are severe, $1/\beta$ should ultimately approach the spacing $\mu/2$ between the Poisson-nucleated cracks and no remnant of the primary-crack nucleation process will remain. The entire distribution would then be a power-law form, as we indeed observe at high velocities in this work.

In this regime, the only variation between fragmentation events will be in the damping length $1/\beta$, which will still vary with a number of factors. The value μ for main-crack nucleation will itself decrease in some characteristic way with the strain-rate. Additionally, the microbranching length is expected to have a dependence on the crack velocity, which may vary spatially throughout the sample in complex impact events. Based on the previous work, we would expect two velocity dependent features; below a certain critical velocity the cracks will not branch, and above this point they should show an approximately linear velocity dependence.[22,30] This leads

us to introduce the following form for the damping length at or above the critical crack velocity:

$$\frac{1}{\beta(v)} = \frac{\mu}{2}\left(\frac{v - v_c}{c_R}\right), \tag{5}$$

where v is the crack velocity, μ is the characteristic length scale from primary crack nucleation, v_c is the critical onset velocity for microbranching, and $v_c \approx c_R/3$ where c_R is the Rayleigh wave speed.[20,21]

As an estimate for β, one might examine low strain-rate experiments (such as dropping or plate-smashing experiments which are common in studies of brittle fragmentation) and use the characteristic Poisson length from this, scaled to higher strain-rates, to estimate the upper bound of $1/\beta$. Alternatively, one could directly estimate the average fragment size μ using an existing theoretical expression such as that derived by Levy and Molinari[32] or the energy-balance relation derived by Grady.[6] The latter takes the form

$$\mu = \left(\frac{\sqrt{12}K_f}{\rho c \dot{\epsilon}}\right)^{\frac{2}{3}}, \tag{6}$$

where ρ is the density, c is the sound speed, $\dot{\epsilon}$ is the strain rate, and K_f is a dynamic fragmentation toughness. In Figure 6, the shaded region shows an estimated range of values for $1/\beta$ in this experiment using Eqs. (5) and (6). For reasonable values of K_f (1 MPa $m^{\frac{1}{2}}$) and $\dot{\epsilon}$ (10^3 to 10^4 s^{-1}) for our materials and impact conditions, Eqs. (5) and (6) yield a maximum value for $1/\beta$ of approximately 0.5-2 mm, in line with what is observed experimentally. The sphere will experience a range of strain rates and crack velocities, but as an initial attempt this method appears promising as a simple means of estimating an average β.

Overall, the trend for β observed in this work is consistent with the idea that microbranching is governing this parameter, though clearly a fragment distribution alone cannot fully confirm this. At the lowest impact velocities, the process is dominated by an exponential distribution, but there is still a small component of the power law form and $1/\beta$ extends into a very small region away from the crack. The larger impact velocities have larger values of $1/\beta$, again consistent with an increasing size of the microbranching region at higher strain rates. The cutoff is larger for the 1220 m/s experiments than for the 1829 m/s ones; if we assume that the entire material is already being fragmented into a power-law distribution by the microbranch damage zones at the intermediate velocity, then this reduction at the highest velocity could be explained by a decrease in the main-crack spacing μ with increasing strain rate.

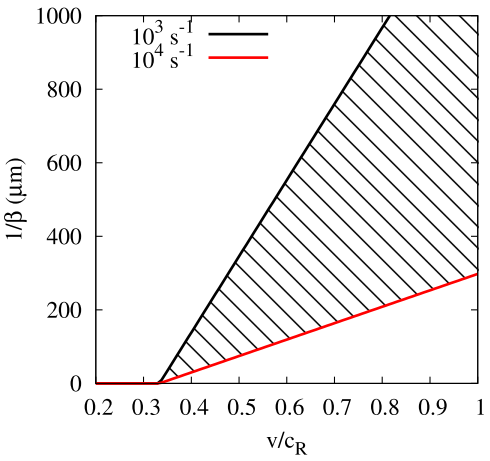

FIG. 6. The shaded region represents approximate lengths of microbranches, incorporating both the crack-velocity dependence (Eq. (5)) and the strain-rate dependence of the average main crack spacing (Eq. (6)).

Many pressed, granular composites similar to the basic aluminum material, discussed here, are currently being considered as reactive material formulations.[1,23] The existence of a power-law fragment distribution at high impact velocities has important implications for the combustion of these materials. In particular, the distribution at high strain-rates will be heavily biased towards very small metal particulate, which will combust rapidly but provide little ability to penetrate additional material. Standard ductile metals exhibit the opposite behavior: non-combustible fragments are centered around a large characteristic length scale. Optimizing the dynamic fracture toughness and strain-rate dependent fragment distribution of reactive materials between these two regimes will be critical for their practical implementation.

IV. CONCLUSIONS

In summary, we report the fragment distributions obtained following impact of brittle, cold-pressed aluminum reactive materials at velocities of 610, 1220, and 1829 m/s on thin steel plates. Fragments were recovered from a soft-catch apparatus and analyzed down to a scale of 44 μm. With increasing velocity, we observe a transition in the character of the fragment distribution from an exponential to a power-law form. A normalized power-law distribution with a finite size cutoff is introduced and used to analyze impacts at the two higher velocities. The exponent of the power-law behavior is very close to the universal value discussed in the recent work. At the lowest velocity, a combined fragment distribution is used, containing both an exponential type form (specifically, the Mott distribution) and a simplified power-law term. The finite size cutoff parameter is consistent with the idea that this quantity is determined by the length of microbranching regions from high-velocity cracks nucleated by a standard Poisson process. At high velocities, the cutoff approaches the average distance between nucleated main cracks, and the entire fragment distribution is, thus, dominated by a single power-law form. For granular materials with very low fracture toughness such as the pressed aluminum considered here, this may be a general behavior and a means of estimating the power-law cutoff parameter for fragmentation at sufficiently high strain rates. The measured fragment distributions provide a basis for future estimates of combustion damage following high velocity impact of reactive materials.

ACKNOWLEDGMENTS

The authors would like to thank Grant Richardson, Richard Lee, and Sam Thuot for technical work setting up the

shots and sieving the fragments, and Jason Jouet and Amy Lees for useful discussions. This work was supported by the Defense Threat Reduction Agency via the Advanced Energetics Initiative and by the Office of Naval Research's Reactive Materials program.

[1]R. G. Ames, MRS Proceedings **896**, 0896-H03-08 (2005).
[2]E. B. Herbold, V. F. Nesterenko, D. J. Benson, J. Cai, K. S. Vecchio, F. Jiang, J. W. Addiss, S. M. Walley, and W. G. Proud, J. Appl. Phys. **104**, 103903 (2008).
[3]J. Nable, A. Mercado, and A. Sherman, MRS Proceedings **896**, 0896-H01-03 (2005).
[4]H. Wang, Y. Zheng, Q. Yu, Z. Liu, and W. Yu, J. Appl. Phys. **110**, 074904 (2011).
[5]D. Grady and M. Kipp, J. Appl. Phys. **58**, 1210 (1985).
[6]D. Grady, *Fragmentation of Rings and Shells* (Springer, New York, 2006).
[7]N. F. Mott and E. H. Linfoot, Ministry of Supply Report No. AC3348, 1943.
[8]L. Oddershede, P. Dimon, and J. Bohr, Phys. Rev. Lett. **71**, 3107 (1993).
[9]J. A. Aström, F. Ouchterlony, R. P. Linna, and J. Timonen, Phys. Rev. Lett. **92**, 245506 (2004).
[10]G. Timar, J. Blomer, F. Kun, and H. J. Herrmann, Phys. Rev. Lett. **104**, 095502 (2010).
[11]A. Diehl, H. A. Camona, L. E. Araripe, J. S. Andrade, and G. A. Farias, Phys. Rev. E **62**, 4742 (2000).
[12]S. Levy, J. F. Molinari, L. Vicari, and A. C. Davison, Phys. Rev. E **82**, 066105 (2010).
[13]A. Levandovsky and A. C. Balazs, Phys. Rev. E **75**, 056105 (2007).
[14]H. A. Carmona, F. K. Wittel, F. Kun, and H. J. Herrmann, Phys. Rev. E **77**, 051302 (2008).
[15]J. A. Aström, Adv. Phys. **55**, 247 (2006).
[16]J. A. Aström, R. P. Linna, J. Timonen, P. F. Moller, and L. Oddershede, Phys. Rev. E **70**, 026104 (2004).
[17]E. Sharon and J. Fineberg, Phys. Rev. B **54**, 7128 (1996).
[18]A. Bershadskii, J. Phys. A **33**, 2179 (2000).
[19]A. Bershadskii, Eur. Phys. J. B **14**, 323 (2000).
[20]E. Sharon, S. P. Gross, and J. Fineberg, Phys. Rev. Lett. **74**, 5096 (1995).
[21]E. Sharon, S. P. Gross, and J. Fineberg, Phys. Rev. Lett. **76**, 2117 (1996).
[22]J. Fineberg and M. Marder, Phys. Rep. **313**, 1 (1999).
[23]S. C. Thuot, J. Wilkinson, R. J. Lee, J. R. Carney, J. Hooper, J. M. Lightstone, J. R. Jouet, and J. G. Rogerson, *in American Institute of Physics Conference Series*, edited by M. Elert, M. D. Furnish, W. W. Anderson, W. G. Proud, and W. T. Butler (American Institute of Physics, Melville, 2009), Vol. 1195, pp. 1011–1014.
[24]Y. Hayakawa, Phys. Rev. B **53**, 14828 (1996).
[25]T. Kadono and M. Arakawa, Phys. Rev. E **65**, 035107 (2002).
[26]A. M. Gaudin and T. P. Meloy, Trans. Soc. Min. Eng. AIME **223**, 40 (1962).
[27]R. Schuhmann, Trans. AIME **217**, 22 (1960).
[28]P. Rosin and E. Rammler, J. Inst. Fuel **7**, 29 (1933).
[29]D. E. Grady, Int. J. Impact Eng. **35**, 1557 (2008).
[30]E. Bouchbinder and I. Procaccia, Phys. Rev. E **72**, 055103 (2005).
[31]E. Bouchbinder, J. Mathiesen, and I. Procaccia, Phys. Rev. E **71**, 056118 (2005).
[32]S. Levy and J. F. Molinari, J. Mech. Phys. Solids **58**, 12 (2010).